BIOFIND:

BIOMAGNETIC FRAMEWORK FOR IDENTIFYING NETWORK DYSFUNCTION IN DEMENTIA

Report of a JPND Working Group on Harmonisation and Alignment in Brain Imaging Methods

April 2018

JPND research

EU Joint Programme – Neurodegenerative Disease Research

CONTENTS

Executive Summary

The principal aim of BioFIND was to define a methodological framework for magnetoencephalography (MEG) to identify sensitive and specific biomarkers of neurodegeneration in Alzheimer's disease (AD) and other dementias. This working group brought together leading international centres for dementia research and brain imaging to establish the optimal paradigms, analyses and standardised reporting methods for MEG dementia research. A large integrated data set created from two separate sites was used to test a mutually agreed pipeline for preprocessing data, and provide direct comparisons of different analytic methods to quantify performance and potential for a future trial-ready platform. This pivotal work provides protocols that are transferable and scalable across multiple sites, enable standardised data sharing, and facilitate large-scale collaborative projects.

Introduction

A major challenge to the development of new mechanistic therapies for dementia is to establish robust biomarkers that can detect and monitor early stages of illness, and which directly reflect the consequences of underlying pathology on neurophysiology and function. Such biomarkers may also be used to understand the emergence of behavioural and cognitive symptoms across major dementia syndromes. Alzheimer's disease (AD), the prodromal state of mild cognitive impairment (MCI), and Frontotemporal lobar degeneration (FTLD), account for the majority of dementia cases and provide the opportunity to test new biomarkers through the contrast between clinical symptoms and pathology.

Magnetoencephalography (MEG) is a promising tool to study neurodegeneration, not only by its proven sensitivity to disease and safety as a non-invasive test, but also by its direct representation of network and synaptic physiology. MEG provides enriched high dimensional data on neuronal activity, oscillatory dynamics, and connectivity at a millisecond time-scale. Critically, the evoked and oscillatory signals can be used to estimate neural interactions between brain regions, which are key to establishing reliable biomarkers of the macroscopic sequelae of neurodegeneration. Brain networks are selectively vulnerable to neural dysfunction, even in preclinical disease (Maestú et al., 2015), and changes in connectivity can predict conversion from MCI to AD (Bajo et al., 2012). A recurrent finding is abnormal neural responses and *hyper*connectivity, observed in MCI and early AD (Bajo et al., 2010; Hillary et al., 2015), that then diminish with advancing disease (Stam et al., 2009) and also observed in FTLD (Hughes et al., 2013). Reorganisation in functional connectivity may be frequency specific, with a dynamic shift in oscillatory power coupling between regions, indexing disease severity in AD/MCI (Stam et al., 2006; Lopez et al., 2014) and FTLD (Hughes et al., 2013). Frequency-specific selective network reorganisation and dysfunction can be used not only to distinguish disease from health, but also discriminate between illnesses (de Haan et al., 2009). Changes in neural oscillations are

considered to have potential as early prognostic biomarkers of dementia; there is clear converging evidence for slowing and reduced alpha power and increased power in lower frequencies, in those with subjective memory complaints and MCI (Garcés et al., 2013, Lopez-Sanz et al., 2016, Gouw et al., 2017).

However, the complexity of MEG data has inspired diverse analytical approaches to assess brain networks; data are characterised along numerous dimensions with different methodological techniques for preprocessing and analysis, and multiple endpoints used to measure the impact of neurodegeneration. This variability in methods hinders direct comparisons between studies and across sites, when it is critically important to understand the common brain responses to damage versus those that are disease specific and potential targets for therapeutic treatment (cf. Hillary et al., 2015). A standardised approach, which harmonises data acquisition and analyses, will facilitate data sharing and provide a core dataset for validation benchmarks in future studies. Frameworks for identifying AD with MEG have been proposed (Zamrini et al., 2011), and we intend to extend this work to include a multi-centre approach with a combination of analytical strategies.

This working group aimed to produce consensus and evidence based guidelines for MEG methodologies for dementia research, including multicentre data acquisition protocols and analysis pipelines. These outputs will support academic and pharma initiatives in dementia research with the crucial tools for stratifying patients and testing future therapeutic treatments.

Methods and Timelines

Four key objectives were identified to reach a consensus framework for MEG and dementia:

1. Identify paradigms to measure candidate biomarkers that are reliable, sensitive and scalable.

2. Evaluate the specificity of MEG biomarkers, and their potential mechanistic insights.

3. Assess multicentre data acquisition / data sharing challenges

4. Establish good practice protocols that optimise sensitivity to the identified biomarkers.

The working group met in November 2016 and July 2017 with multiple discussions via email and smaller meetings throughout the year to write the MEG framework and complete the pilot study.

Timeline for working group

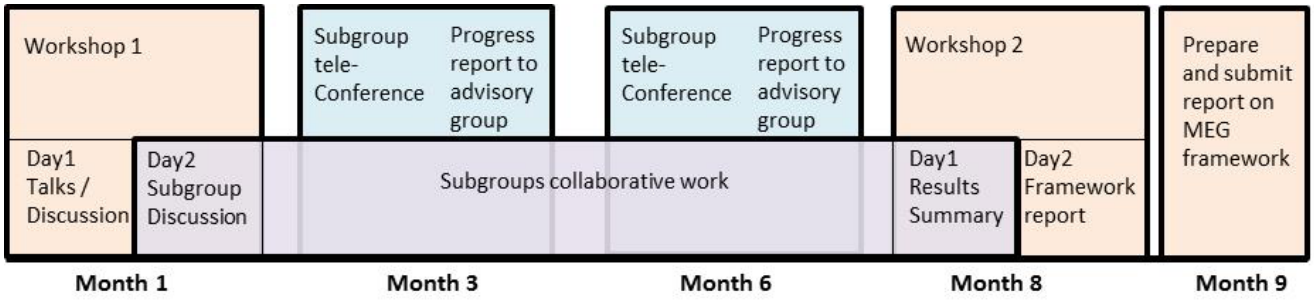

The first meeting comprised a series of presentations and discussions, which addressed each of the objectives. All speakers were asked to respond to two specific questions: 1. What are the key challenges to identifying Biomarkers in dementia? 2. Can we achieve data acquisition and analysis at scale and at the global level?

The presenters provided strong evidence that MEG can indeed be sensitive and specific to AD, other dementias and MCI, with a number of demonstrations of potential biomarkers. There was convergence across groups using a 'resting state' paradigm that revealed a signature of slowing oscillatory brain activity in AD and MCI, which may point towards a marker of disease and disease progression. However there were a number of key challenges raised which make comparing and pooling data from multiple sites complex and methods difficult to transfer between groups.

The steering committee provided views from a pharmaceutical perspective (Stephen Lowe) and from 'big-data' research (Professor Barry Horwitz) to highlight the challenges faced in creating large data sets capable of identifying reliable biomarkers that can be used in clinical trials and to benchmark treatment or disease progression.

Key Challenges

Key challenges of identifying biomarkers of dementia in MEG were raised, including:

- Different biomarkers are needed for different questions: for example detection of dementia, differential diagnosis, progression of disease, efficacy and outcome of treatment strategies, stratification of patients and responder vs. non-responders. Thus multiple analytical methods or paradigms may be required, and a clear question addressed to inform disease biology.
- High variability in methods available: including hardware used, acquisition protocols, types of preprocessing and analysis used, the numerous parameter decisions made within each method.
- Identifying reliable procedures for clinical trials / drug development is difficult due to such variability in methods together with the biological variability of patients. A standardized framework, to reduce methods variance, validated across scientific groups could provide a reliable and reproducible basis for examining potential treatment targets.
- Can MEG methods be scaled for acquisition and analyses on larger patient groups. Multisite studies can provide a higher / faster throughput of data, if data sets can be directly compared and pooled.

Pilot data set

A data set was created to test the standardized framework of data acquisition and analyses across MEG sites, and to further examine a set of methods used to identify potential biomarkers of MCI/AD. A description of the data is in Table 1. Details of the steps taken to create the shared data pool are presented in table 2.

The data were pooled from two main sites[1] (the CBU in Cambridge and CTB in Madrid), and included an eyes-closed resting-state paradigm, from patients with MCI / early AD and age-matched healthy controls. The data were selected by compatibility and shareability: data were acquired on Neuromag MEG, had similar acquisition protocols, similar groups of

[1] N=3 of the Cambridge Patient group were actually scanned at OHBA in Oxford, as part of a shared project. The recruitment procedures matched those for the other Cambridge patients, so these 3 are treated as part of the Cambridge group for demographic and behavioural analyses. For the purpose of covarying out possible site differences in the MEG analyses (since the magnetic environment may differ across sites), OHBA was treated as a third site.

patients/controls and no restrictions in data sharing. Second, an agreed pipeline for preprocessing the data was created (see appendix 3). Finally the data were analysed by each subgroup using the preferred methods and presented at the second meeting. Subgroups were split by location: Cambridge, Madrid and Oxford.

Two main restrictions that deviate from the initial proposal were to include only MEG (and not EEG) from patients with MCI (and not including patients with FTLD). The MEG data sets were considered more compatible for pooling, and have the advantage of a much richer data set than EEG, with greater potential for reliability and validity of results. The pooled data set was restricted to MCI patients to include compatible data from multiple sites. The aim of direct comparisons with frontotemporal dementia is confirmed for a later stage to be undertaken in 2018.

Data Details

For the "Cambridge" data, N=42 patients were recruited following a MCI diagnosis from a local neurologist, as part of several ongoing projects led by Henson (n=29) and Hughes (n=13). Some (n=8) of the patients tested by Hughes were recruited as part of the 'Deep & Frequent Phenotyping Pilot (DFP) Study' led by Rowe. All were scanned at the CBU in Cambridge, apart from n=3 of the DFP study, who were scanned at OHBA in Oxford.

The N=42 controls were selected from the population-representative CamCAN database (http://camcan-archive.mrc-cbu.cam.ac.uk), so as to be age- and sex-matched to the patients.

For the "Madrid" data the total sample (N=42 patients and N=42 Controls) was recruited from the Neurology and Geriatric Departments of the University Hospital San Carlos (Madrid, Spain), from the Centre for Prevention of Cognitive Impairment (Madrid, Spain) and the Seniors Center of Chamartin District (Madrid, Spain). All the subjects were right handed (Oldfield, 1971) and native Spanish speakers.

MCI diagnosis was established according to the National Institute on Aging–Alzheimer Association (NIA–AA) criteria (Albert et al., 2011): (1) self- or informant-reported cognitive complaint; (2) objective evidence of impairment in one or more cognitive domains; (3) preserved independence in functional abilities; and (4) not demented (McKhann et al., 2011).

All participants were asked “Please close your eyes and keep them closed and try to relax and stay still for the duration of the recording. This will take about five minutes”. What participants had been doing before the eyes-closed recording varied depending on the project that they were recruited for, and is a potential source of unmodelled variance, contributing to, for example, tiredness. Drowsiness was also monitored before and after the recording (by asking participants how they were feeling) to ensure they stayed awake.

All MEG data (from all 3 sites) were recorded on an Elekta VectorView system with 102 magnetometers and 204 planar gradiometers.

The Cambridge MRIs were from 1mm3 isotropic T1-weighted MPRAGE sequences run on a Siemens 3T Trio or Prisma at the CBU and OHBA. 4 Cambridge patients did not have MRIs available. The MRI’s acquired in Madrid were T1-weighted, acquired in a General Electric 1.5 Tesla magnetic resonance scanner, using a high-resolution antenna and a homogenization PURE filter (Fast Spoiled Gradient Echo sequence, TR/TE/TI=11.2/4.2/450 ms; flip angle 12°; 1 mm slice thickness, 256×256 matrix and FOV 25 cm).

Table 1. Data sample included in pilot study.

	Madrid		Cambridge		All	
	Controls	Patients	Controls	Patients	Controls	Patients
N	42	42	42	42	84	84
Sex (M/F)	19/23	19/23	28/14	28/14	47/37	47/37
Age	72.3 (2.7)	72.2 (3.3)	69 (8)	69 (8)	70.8 (6.1)	70.8 (6.2)
MMSE	29.0 (1.1)	26.9 (2.8)	28.8 (1.2)	25.1* (3.1)	28.9 (1.1)	26.0 (3.1)

* Two patients from Cambridge group had missing MMSE scores

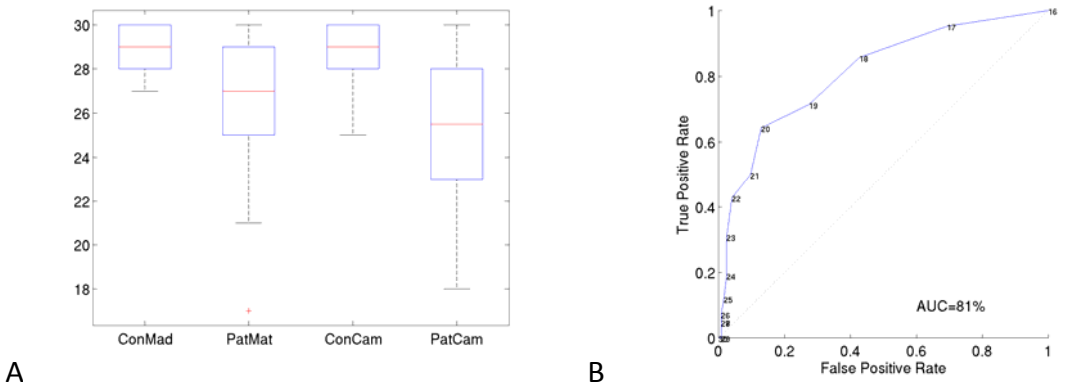

A B

Figure 1. A) Distribution of MMSE scores (max=30) for each Group (Con=Control; Pat=Patient) and Site (Mad=Madrid; Cam=Cambridge; OHBA patients included with Cambridge since recruited same way). B) ROC after adjusting for age, sex and Site.

There were more women than men in the Madrid group, and more men than women in the Cambridge group. Sex was used as a covariate in imaging analysis below.

A 2 (Group: Control vs Patient) x 2 (Site: Cambridge vs Madrid), between-subject ANOVA was performed on Age and MMSE score. For Age, though there was a significant main effect of Site, $F_{(3,164)}$=10.3, p=.002, with the Madrid group older, there was no significant main effect of Group, or interaction between Group and Site, Fs<1. Age was used as a covariate in imaging analyses below.

For MMSE (excluding the two missing scores), there was the expected main effect of Group, $F_{(3,162)}$=70.9, p<.001, with patients scoring lower than controls. There was also a main effect of Site, $F_{(3,162)}$=7.44, p=.007, with Cambridge site having lower scores, and an interaction, $F_{(3,162)}$=5.67, p=.018, with the control-patient difference being larger from the Cambridge site. There was a considerable spread and negative skew for the patients (Figure 1A).

For a reference to the imaging analyses below, an ROC was performed on the N=166 MMSE scores for distinguishing controls from patients (Figure 1B), which revealed an overall Area Under the Curve (AUC) of 81% (a balanced accuracy of 75%), regardless of whether MMSE scores were adjusted for age, sex and site.

Subgroup Results

CAMBRIDGE

MRIs

The T1-weighted MRIs were initially coregistered to the MNI template using a rigid-body transformation, and then segmented into 6 tissue classes: GM, WM, cerebrospinal fluid (CSF), bone, soft tissue, and residual noise using SPM12. The GM images were then submitted to diffeomorphic registration (DARTEL) to create a group template image, which was then affine-transformed to the MNI template. To accommodate changes in volume from these transformations, the GM images were modulated by the Jacobean of the deformations to produce estimates in MNI space of the original local GM volume. The resulting images contained 121x145x121 voxels of 1.5mm isotropic resolution, and were finally smoothed by an 8mm isotropic Gaussian kernel.

Mass Univariate (VBM)

There were N=164 participants with MRIs (not acquired on 4 of the Cambridge patients), and for simplicity of analysis, the three patients scanned at OHBA were included with those scanned at the CBU. A voxel-based morphometric (VBM) analysis was run with a General Linear Model (GLM) including Group (Patient/Control) and Site (Madrid/Cambridge) factors, and age and sex as covariates. Inhomogeneity of error variance was modelled and used to prewhiten the GLM and data. Results showed the expected reductions in GM volume in patients, most prominently in bilateral medial temporal regions (Figure 2), as well as medial parietal and some lateral temporal regions. There were also large effect of Site across the whole brain (not shown), but any Site by Group interactions were small and not in regions of significance.

Multivariate Classification (MKL)

The normalised gray-matter images were also used to assess classification performance using Multi-Kernel Learning (MKL) within the PRoNTO v2.0 toolbox (http://www.mlnl.cs.ucl.ac.uk/pronto), with leave-one-out-cross-validation. In addition to the 4 patients without MRI, a further 2 patients were excluded because excessive movement during their MEG scan (see below), so that the same N=162 participants were used for both MRI, MEG and combined MRI-MEG image-based classification (see later). Four

covariates were included: age, sex and binary indicators for whether the site was CTB, CBU or OHBA.

The AUC was 75% (with a balanced accuracy of 68%; see ahead to Figure 8 & 9), less than the MMSE, though of course both MMSE and clinical scans like the T1 MRI (though not exactly the same scans) are part of the evidence used by the clinician to label someone with MCI, so these accuracies are likely to be upward biased (unlike the MEG).

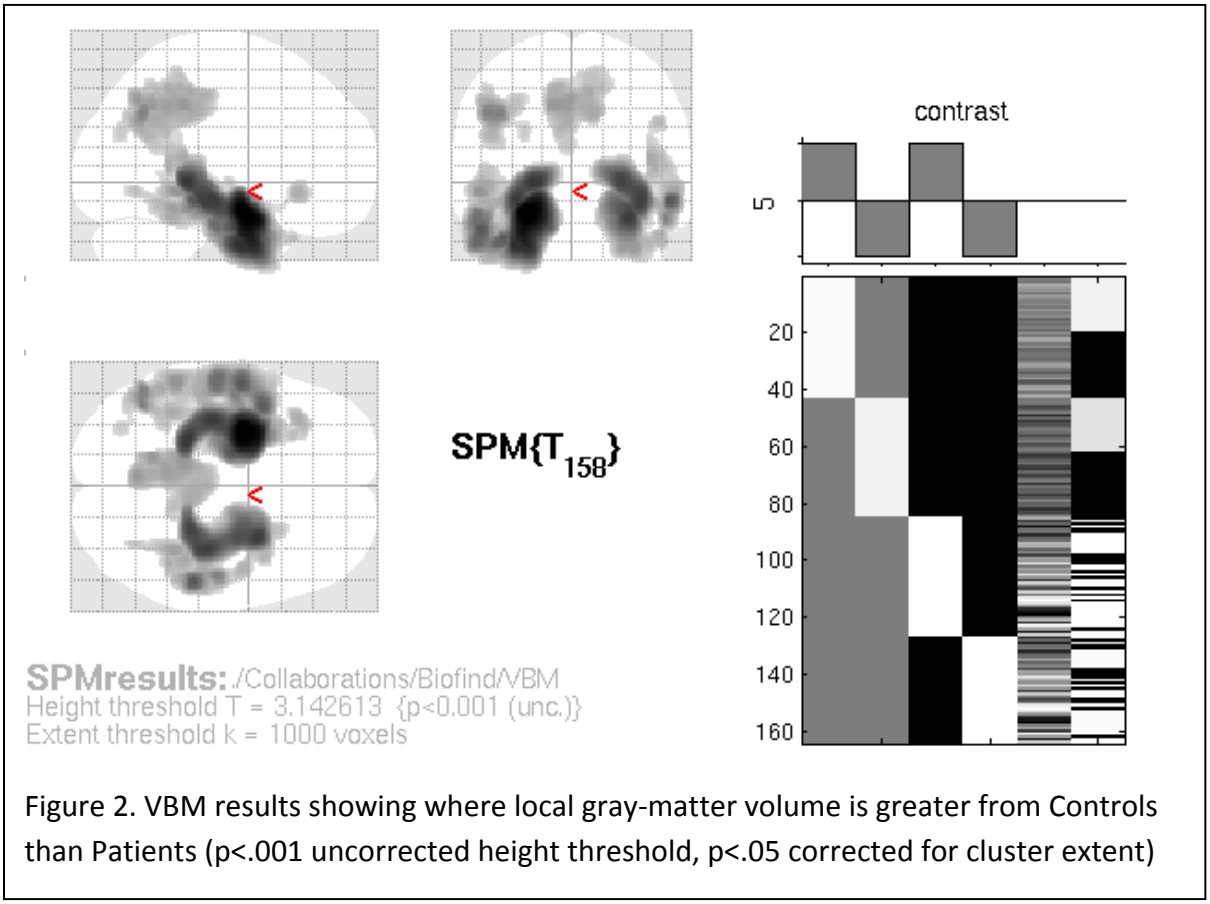

Figure 2. VBM results showing where local gray-matter volume is greater from Controls than Patients (p<.001 uncorrected height threshold, p<.05 corrected for cluster extent)

MEG

Maxfilter

The continuous data were cleaned using the Maxfilter software (v2.2.12). The origin of the SSS expansion was determined by fitting a sphere to all digitized headpoints excluding those around the nose (excluding those with y>0 and z<0). Separate cross-talk and calibration files were used for each of the 3 sites. There were 3 maxfilter steps. In the first step, bad channels were detected (those that maxfiltered reported as bad in more than 5% of the 4s

epochs[2]) and movement parameters written every 1s. In the second step, the data were cleaned using the temporal extension of SSS (10s windows with a correlation of 0.9 recommended by Madrid), with bad channels defined from the first step. The data were also corrected for head motion every 1s, except for 11 Madrid participants (8 patients) and 1 Cambridge control from whom movement correction failed (owing to loss of HPI coils). Mains noise at 50Hz and harmonics were attenuated. In the final step, the data were transformed into common device space, by aligning the head and device axes, and setting the head centre to [0 13 -6] in device coordinates.

Distributions of MaxFilter outputs are shown in Figure 3, and mean values in Table 2. The OHBA group were excluded from statistics, given that only 3 patients, resulting in a 2 (Group: Control vs Patient) x 2 (Site: Cambridge vs Madrid), between-subject ANOVA.

Table 2. Maxfilter and epoch information.

	CTB (Madrid)		CBU (Cambridge)		OHBA (Oxford)	
	Controls	Patients	Controls	Patients	Controls	Patients
N	42	42	42	39	-	3
Bad channels	7.38	6.93	4.64	6.07	-	4.33
Mean Move (mm)	0.80	1.10	0.61	0.94	-	3.15
SD Move (mm)	0.18	0.30	0.06	0.24	-	3.04
Position (mm)	10.5	12.0	10.0	12.9	-	13.9
Time of day (24h)	12.0	11.6	14.2	14.0	-	13.5
Data Onset (s)	250	234	125	132	-	124
Data Offset (s)	419	404	298	306	-	294
No. of Epochs	38.2	39.7	39.8	37.8	-	33.0

[2] NB This step differs from the analyses run in Madrid who identified bad channels by visual inspection.

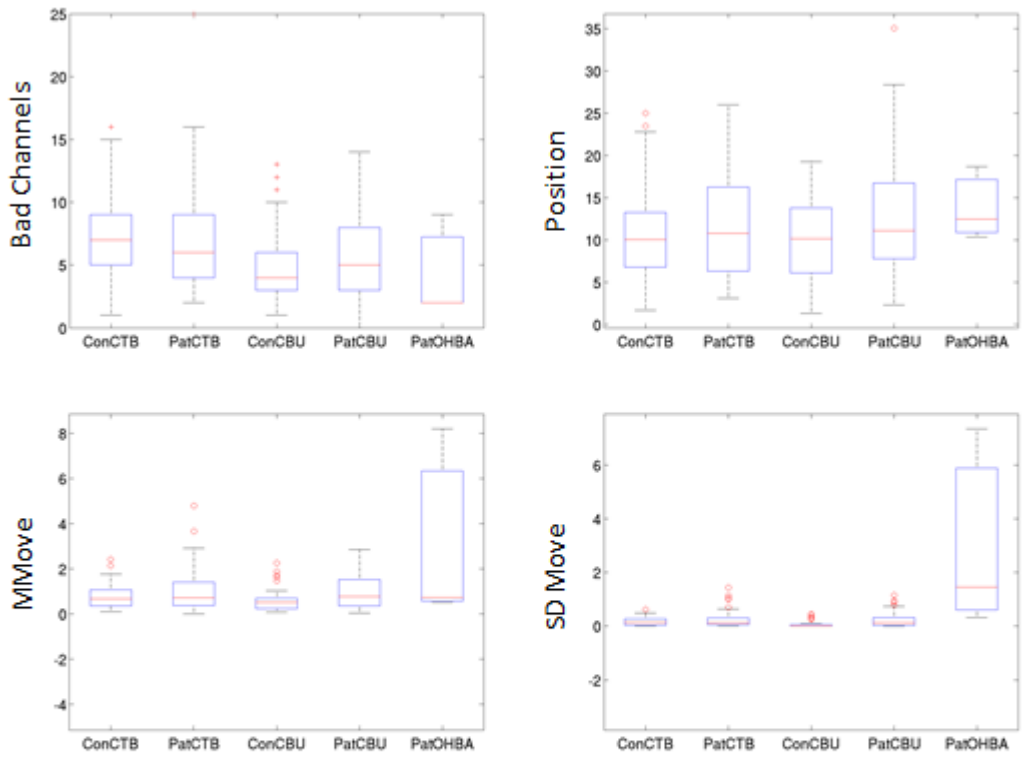

Figure 3. Maxfilter outputs: number of bad channels (Bad), distance between the head centre and device centre (Position), mean within-session translation (MMove) and standard deviation of within-session translation (SDMove). NB OHBA group included only 3 patients.

The number of bad channels showed no difference between Groups, F<1, though more bad channels for CTB than CBU, $F_{(1,163)}$=13.5, p<.001 (and no significant interaction, $F_{(1,163)}$=1.11, p=.29).

Head motion was summarised by the mean and the standard deviation (SD) of translations over the recording. Excluding the 12 participants for whom head motion could not be estimated, there was significantly more mean movement, $F_{(1,151)}$=4.96, p<.05 in the patients, but no difference between sites, $F_{(1,151)}$=1.52, p=.22 or interaction, F<1. The same pattern was seen for the SD of translations, with a borderline group difference, $F_{(1,151)}$=3.36, p=.07, but no difference between sites, $F_{(1,151)}$=1.20, p=.27 or interaction, F<1.

The translation between the head centre and device centre ("Position" in Table 2) was significantly greater for the patients, $F_{(1,163)}$=5.10, p<.05, but did not differ by, or interact with, site, F<1.

Other characteristics of the MEG data are shown in Figure 4 (and summarised at end of Table 2).

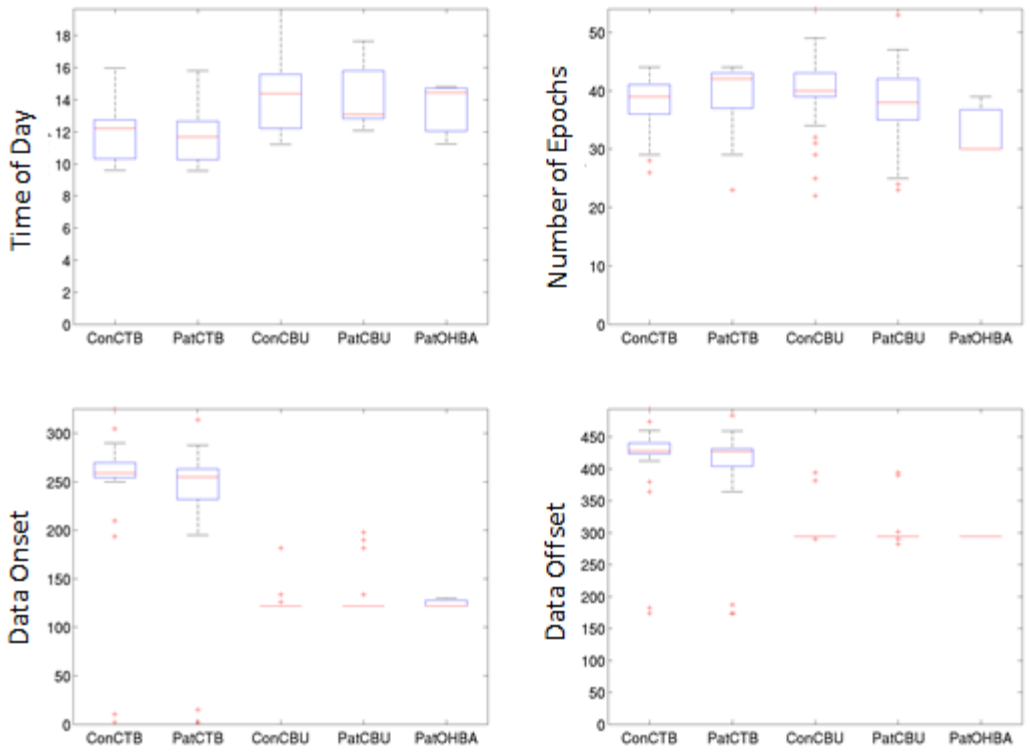

Figure 4. Other MEG Data Characteristics: Time of Day, Number of valid epochs (NumEpochs), start of first epoch (DataOnset) and end of last epoch (DataOffset).

The time of day in which the MEG data were acquired did not differ between Groups, $F_{(1,163)}$=1.07, p=.30, but was later for CBU than CTB sites, $F_{(1,163)}$=66.1, p<.001 (with no interaction, F<1).

The continuous data were divided into multiple 4s epochs that were judged to be artefact-free according to visual inspection of data maxfiltered by the Madrid researchers ("valid" epochs). The start of these epochs within the recording was later in the CTB than CBU data, because the CTB participants performed other tasks prior to rest within the same recording (whereas at the CBU, any previous tasks were run as separate recordings). Importantly, the groups did not obviously differ within each site with respect to either start or end of valid data (Figure 5).

The number of valid epochs did not show main effects of Group or Site (Fs<1), though there was an interaction between these factors, $F_{(1,163)}$=4.22, p<.05, with numerically more valid epochs for patients than controls at CTB site, but vice versa at the CBU site.

Processing in SPM

The maxfiltered files were read into Matlab via SPM12 and epoched into valid epochs. The data within each epoch were then filtered using a fast Fourier transform with multiple Hanning tapers, as implemented by FieldTrips "mtmfft" function, for frequencies from 1 to 92Hz in steps of 0.25Hz. The frequency resolution increased approximately exponentially with mean frequency. The resulting power spectra were averaged over each epoch and the (base 10) logarithm taken. The frequencies were then sub-sampled approximately logarithmically as: every 0.25Hz from 1-14Hz, every 0.5Hz from 14-21 Hz, every 1 Hz from 21-30 Hz, every 2Hz from 30-48Hz and every 4Hz from 52-92Hz.

Two patients (one from CBU, one from OHBA) were excluded for a large distance from centre of helmet (>30mm) and excessive motion (>6mm) respectively (see Figure 3).

The mean power spectra (absolute power) for each Group and Site (excluding OHBA because too few participants to estimate mean accurately), averaged across sensors of a given type, are shown in Figure 5. Patients showed higher power in lower frequencies (up to approximately 16Hz). There was also large effect of Site, with more power overall for the CTB site, and a suggestion of a Site-by-Group interaction with higher power for patients than controls above approximately 25Hz for the CBU but not for CTB.

We examined mean power within Alpha (6-12Hz) and Theta (4-7Hz) bands, as well as their ratio and the frequency of the Alpha peak (Figure 6), based on prior evidence that the latter relate to wakefulness (the peak was identified after smoothing with a 6-frequency bin average).

The AUC (after adjusting for Site, now including OHBA, as well as age and sex) was highest when based on Theta power (71% for both magnetometers and gradiometers), less for Alpha power (63% for magnetometers and 64% for gradiometers) and Alpha peak frequency (63% for magnetometers and 62% for gradiometers) and least for Alpha-Theta ratio (62% for magnetometers and 51% for gradiometers; the latter most likely because Theta log-power values were close to zero, rendering the ratio unstable).

When additionally adjusting data first for bad channels, movement (mean and std) and distance from origin, these figures dropped to: Theta power (mag/grd) 67%,67%; Alpha power (mag/grd) 60%,61%; Alpha Freq (mag/grd) 60%,59%; Alpha:Theta power (mag/grd) 59%,53%

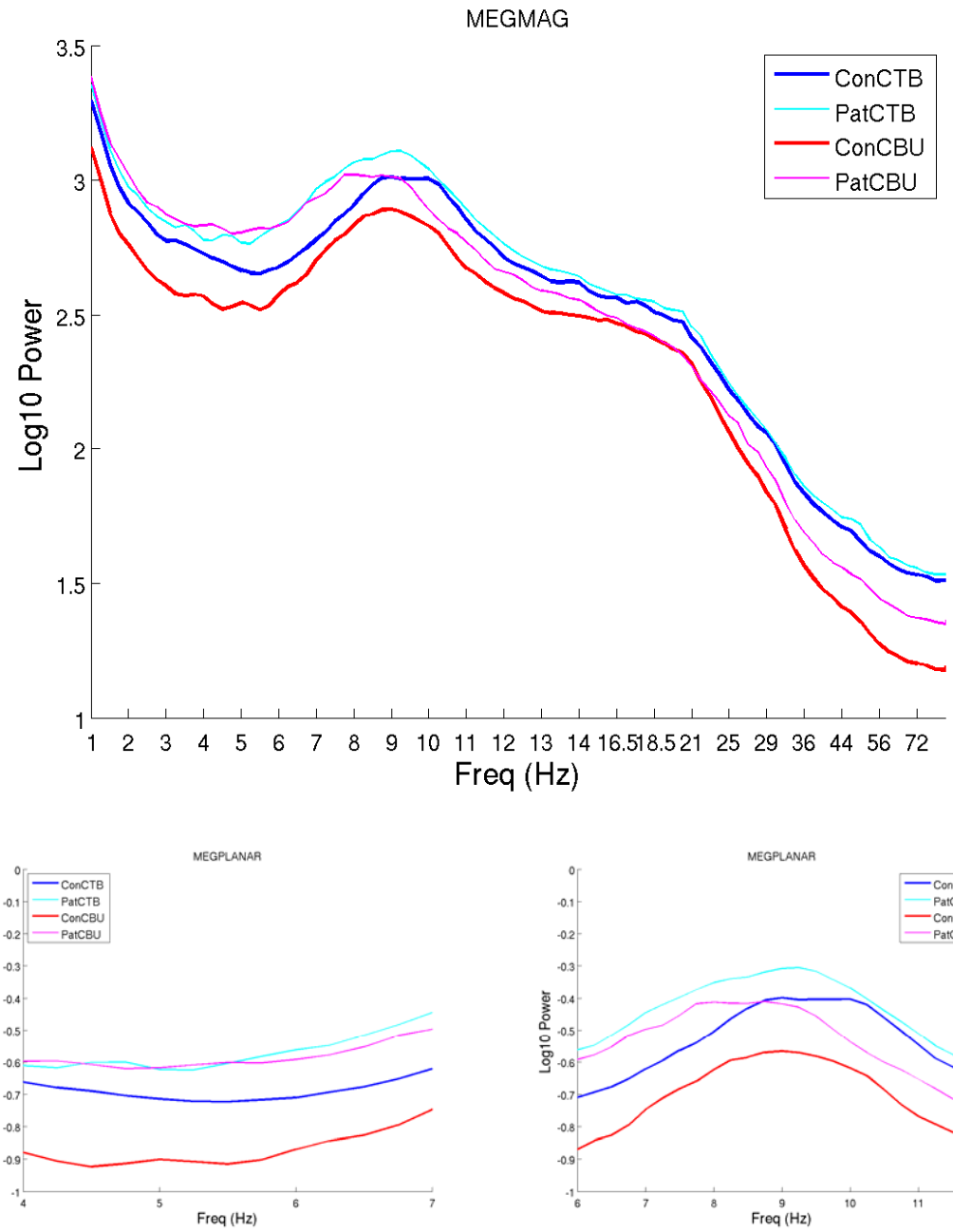

Figure 5. Power spectra for magnetometers for all frequencies (top), and for gradiometers within Theta (bottom left) and Alpha (bottom right) bands. (Other sensor types similar in all cases).

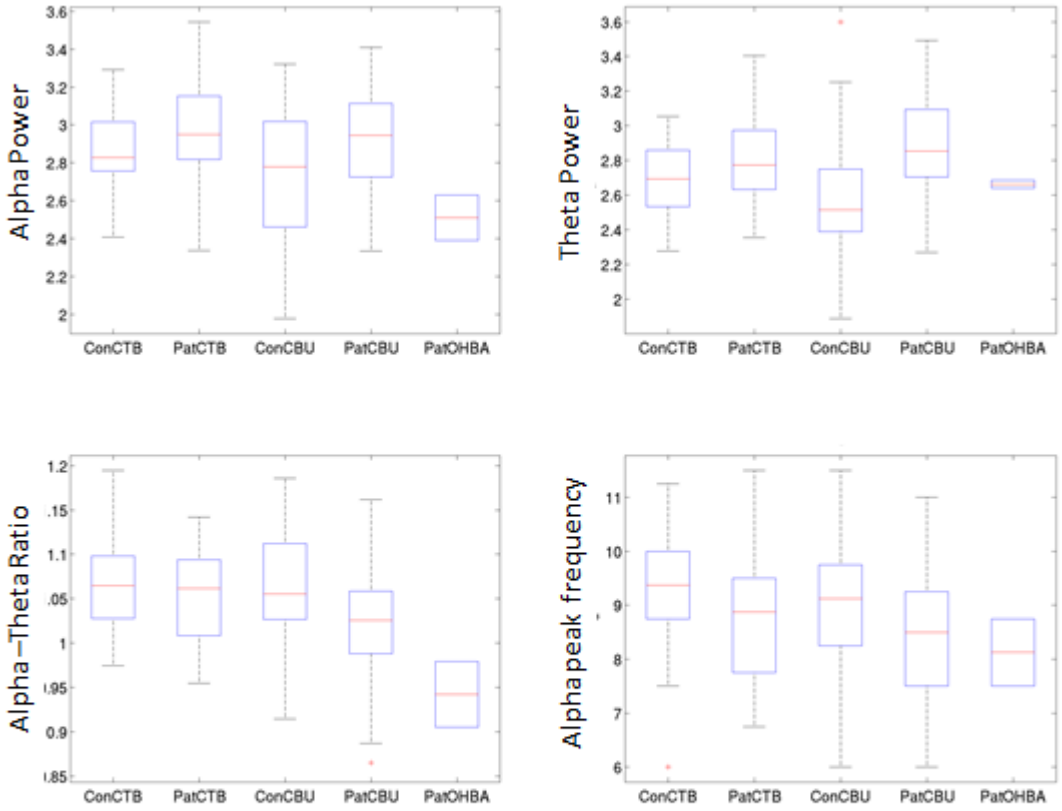

Figure 6. Distribution of Alpha Power (top left), Theta Power (top right), Alpha-Theta ratio (bottom left) and Alpha peak frequency (bottom right) for magnetometers. Gradiometers were similar, except for the Alpha-Theta ratio which was unstable owing to Theta power values close to 0.

Mass Univariate (Scalp-frequency)

The topographic distribution of the group and site differences in power were tested by projecting the sensor locations (either for magnetometers or gradiometers) onto a 32x32 grid and interpolating the data between grid points for each frequency separately, to produce a 32x32x94 3D scalp-frequency image. These images were smoothed in the frequency dimension a 2-pixel FWHM Gaussian kernel. The smoothed images for the N=166 participants with valid MEG data were then entered into the same general linear model as for VBM above, with age and sex covariates. Consistent with above findings, the gradiometers in patients showed greater power in frequencies around the theta range (peaking at 5.5Hz), which was maximal over lateral temporal regions (Figure 7). They also showed greater power at around 52Hz over the centre of the scalp. Controls did not show significantly greater power anywhere. There were also significant main effects of Site over much of the space, particularly higher frequencies over frontal scalp regions, while Site-by-

Group interactions were confined to two smaller clusters over posterior scalp centred at 2.5Hz and at 72 Hz.

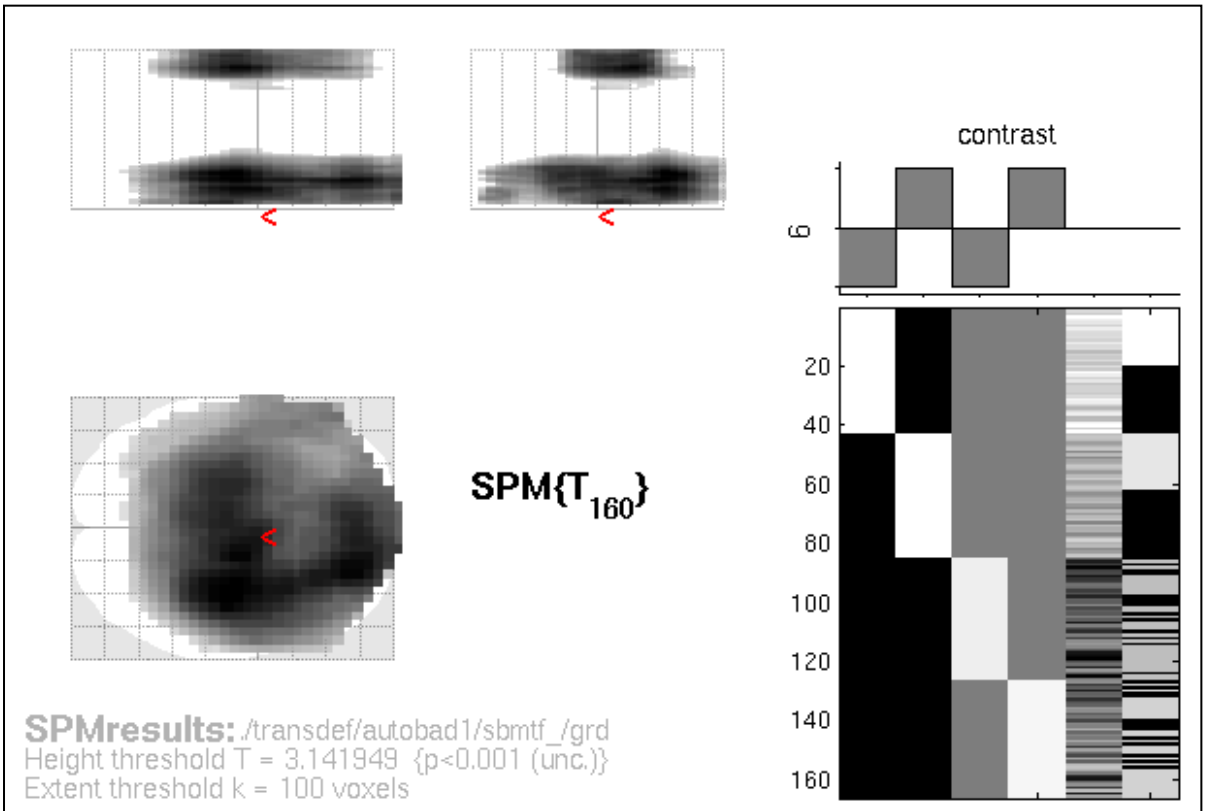

Figure 7. Scalp-frequency results for gradiometers for Pat>Con (p<.001 uncorrected height threshold, p<.05 corrected for cluster extent)

Multivariate Classification (MKL)

The smoothed scalp-frequency images were also used to assess classification performance using MKL, for the same N=162 participants used for the MRI MKL analysis above. Four covariates were included: age, sex and binary indicators for whether the site was CTB, CBU or OHBA.

The AUC was 61% for magnetometers (balanced accuracy of 59%; Figure. 8A) and 71% for gradiometers (balanced accuracy of 66%; Figure 8B), slightly worse than for the MRI (75%, Figure 8C). MRI together with MEG had an AUC of 79% (Figure 9).

Combined Multivariate Classification (MKL) of MRI and MEG

Finally, we combined the MRI gray-matter images with the magnetometer and gradiometer scalp-frequency images in a multi-kernel classifier with 3 kernels. The AUC for this multimodal classification was 79% with balanced accuracy of 76%, better (numerically at least) than for any one modality alone (Figure 9), and comparable to MMSE. Of course, this is just using MEG power as a feature of interest – higher MEG classification might result with other metrics, such as connectivity.

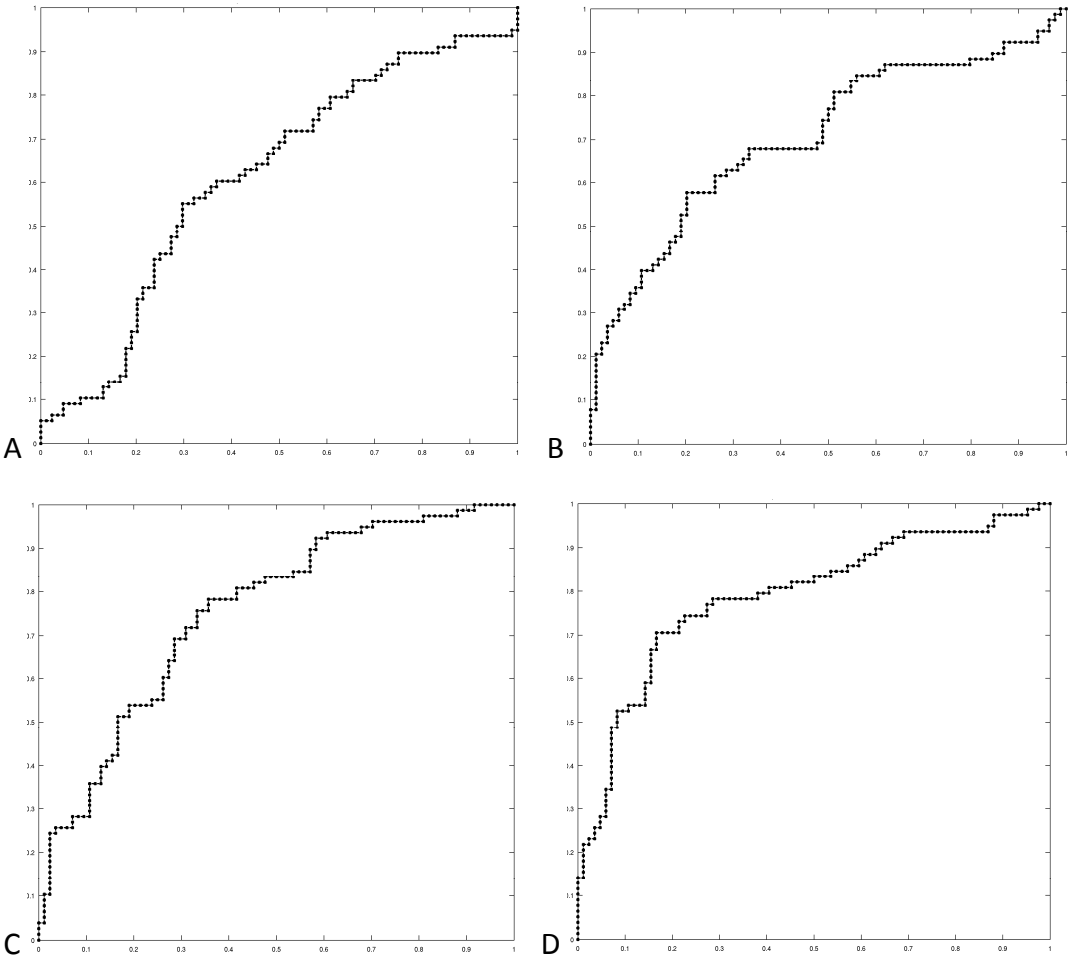

Figure 8. ROCs from MKL image-based classification for magnetometers (A), gradiometers (B), MRI gray-matter (C) and combined magnetometers, gradiometers and MRI (D).

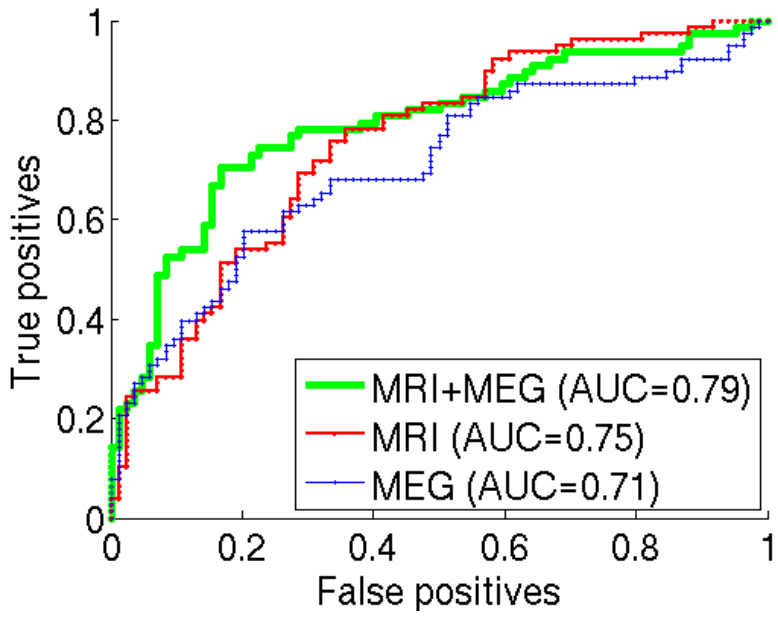

Figure 9. ROCs from MKL image-based classification for MEG (blue), MRI gray-matter (red) and combined MEG and MRI (green).

MADRID

Materials and methods.

MEG acquisition and preprocessing.

Biomagnetic data were acquired using a 306-channel Elekta Vectorview system (Elekta AB, Stockholm, Sweden) placed inside a magnetically shielded room (*VacuumSchmelze* GmbH, Hanau, Germany) located at the Laboratory of Cognitive and Computational Neuroscience (Madrid, Spain). MEG signals were recorded while the subjects were awake, sitting comfortably and with their eyes closed. If a subject reported feeling sleepy during the session, they were given sufficient time to feel more awake and the recording performed again.

Prior to the recording, two electrodes were placed above and below the left eye, in a bipolar montage, to acquire electro-oculographic activity. In addition, four head position indicator (HPI) coils were placed in the head of the subject, two in the forehead and two in the mastoids. The position of the 3 fiducial points, along with the HPI coils and over 200 evenly

spaced points of the head shape of the subject, were acquired using a three-dimensional Fastrack digitizer (Polhemus, Colchester, Vermont). The HPI coils were fed during the whole acquisition, allowing for offline estimation of the head position.

4 minutes of resting state activity were acquired from each subject. Data was online filtered between 0.1 and 330 Hz, and digitized using a sampling rate of 1000 Hz. After the acquisition, recordings were processed offline using the spatiotemporal extension of the signal separation algorithm (tSSS) (Taulu and Simola, 2006). Parameters for the tSSS consisted of a window length of 10 seconds and a correlation threshold of 0.9. This algorithm removes the signals whose origin is estimated outside the MEG helmet, while keeping intact the signals coming from inside the head. In addition, the continuous HPI acquisition, combined with the tSSS algorithm, allowed for the continuous movement compensation. As result, the signals used in the next steps come from a set of virtual sensors whose position remains static with respect to the head of the subject. Data from subjects whose movement during the recording was larger than 25 mm were discarded, following the recommendations of the manufacturer.

MEG data were examined using the automatic artifact detection of FieldTrip toolbox (Oostenveld et al., 2011), looking for ocular, muscular and jump artifacts. A MEG expert, to correct both false positives and negatives, confirmed the detected artifacts. Muscular and jump artifacts were marked and segments containing them were completely discarded. On the remaining segments, a blind source separation algorithm based in second order statistics (SOBI) was used to obtain statistically independent components. SOBI components were labeled as oculographic, cardiographic, noisy components or real data. Artifact-related components were eliminated, and segments containing persistent oculographic artifacts were removed. Last, data was segmented in 4-seconds epochs of artifact-free data. Data with less than 20 epochs were discarded from the analysis, due to a low signal to noise ratio.

Source reconstruction.

A volumetric and regular grid with 1-cm spacing was generated for the MNI template (with one source placed in (0, 0, 0) in MNI coordinates). Only sources inside the brain surface (as defined in the previous section) were taken into account, resulting in a source model with 2459 sources, each consisting in three perpendicular dipoles. Anatomical labels were assigned to each source according to two anatomical atlases: the automatic anatomical labeling (AAL) atlas (Tzourio-Mazoyer , 2002) and a reduced version of the Harvard-Oxford atlas (Desikan et al., 2006; López et al. 2017). The final number of sources considered depended on the atlas, as only cortical sources as well as hippocampal and parahippocampal ones were used: 1467 for the AAL atlas and 1489 for the HO atlas.

A T1-weighted MRI was acquired for each subject. Using this image, the MNI defined grid was transformed to subject space. In addition, a binary mask for the subject brain was

generated using those voxels whose combined probability of WM, GM and CSF were greater than 0.5. Last, a mesh surface was generated from the previous mask using FieldTrip. Finally, both the grid and the brain surface were manually realigned to Neuromag coordinate system using the three fiducials and the head shape as guides. A lead field was calculated using a realistic single shell head (Nolte, 2003) as forward model.

Data was filtered in the classical bands (theta, 4-8 Hz; alpha, 8-12 Hz; beta, 12-30 Hz; gamma, 30-45 Hz and broad band, 2-45 Hz) using a 2000th order FIR band-pass filter designed with a Hanning window. 2 seconds (2000 samples) of real data were used as padding in each side, and discarded after the filtering. The source reconstruction was performed using a Linearly Constrained Minimum Variance (LCMV) beamformer (Van Veen et al., 1997) for each band. The resulting spatial filters were projected over the maximal radiation direction, getting only one filter per source. Then, source-space time series were reconstructed and grouped according to the atlas, obtaining one representative time series for area using (1) the PCA (principal component analysis) of all the sources in the area or (2) the source closest to the centroid of the area.

Spectral analysis.

MEG power spectra between 2 - 45 Hz were calculated for each of the 2459 sources in each clean segment, and then averaged across trials. We employed a multitaper method using discrete prolate spheroidal sequences as tapers and 0.5 Hz smoothing. Power spectra were normalized by the overall power between 2 - 45 Hz. This procedure has been previously detailed elsewhere (López-Sanz et al., 2016).

Power statistics

Relative power in each classical frequency band was compared with a 2-way ANOVA using diagnostic (MCI vs CN) as the main factor and the center (Madrid vs Cambridge) as a covariate. Multiple comparisons were controlled using Cluster Based Permutation Test (CBPT) and using $\alpha = 0.05$ for cluster thresholding.

Frequency Results

Delta band (2 - 4 Hz)

Patients with MCI showed increased relative delta power in a cluster comprising bilateral brain regions over occipital areas such as cuneus, precuneus and calcarine; widespread bilateral temporal structures including hippocampus and parahippocampal cortices among others and extending into bilateral orbitofrontal areas ($p = 0.01$) (Figure 10A).

Theta band (4 – 8 Hz)

Relative theta band power was significantly increased in MCI patients ($p = 9.9 \cdot 10^{-5}$). Areas affected by theta power increase were distributed across the entire cortical surface, but were more intense over bilateral middle temporal gyri (Figure 10B)

Alpha band (8 – 12 Hz)

MCI patients exhibited a significant decrease in relative alpha power ($p = 0.027$). Alpha disruption affected bilateral temporal cortices. Furthermore, these alterations extended into orbitofrontal regions (Figure 10C).

Beta band (12 - 30 Hz)

Beta band relative power was significantly decreased in MCI patients ($p = 9.9 \cdot 10^{-5}$), although the significant cluster included widespread regions affecting most cortical regions, it was more intense over bilateral temporoparietal areas such as angular gyrus, inferior parietal lobe and middle temporal gyri (Figure 10D).

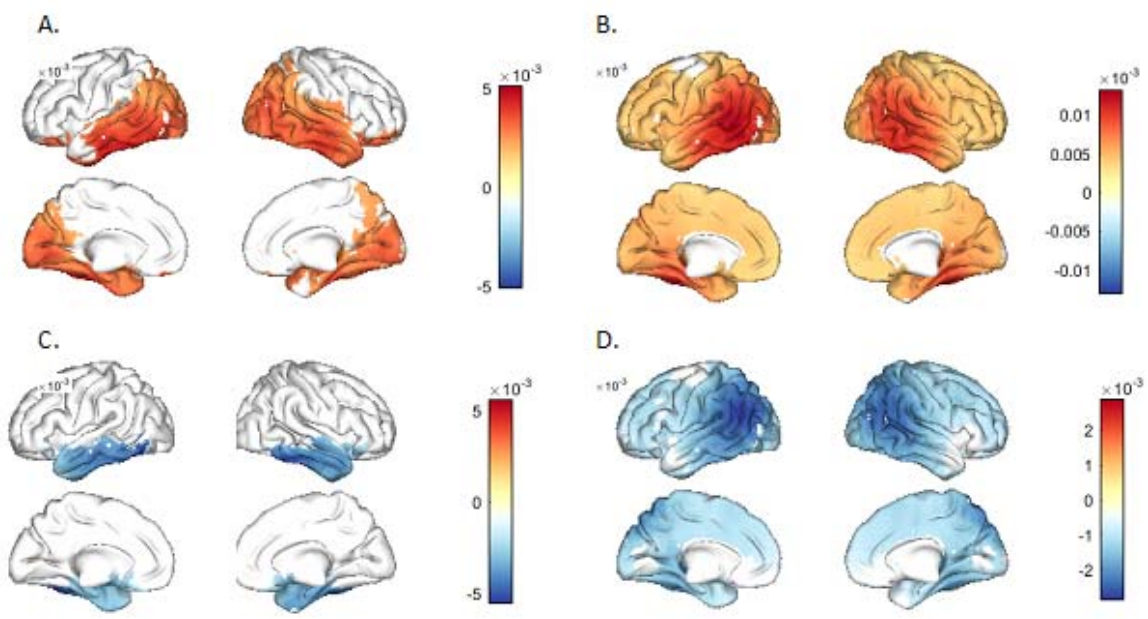

Figure 10. Differences in relative power across frequency bands for patients vs controls. A, Delta band (2 – 4 Hz); B, Theta band (4 – 8 Hz); C, Alpha band (8 – 12 Hz); D, Beta band (12 –30 Hz).

Functional connectivity analysis

Functional connectivity (FC) analyses were performed using Phase Locking Value (PLV) and Mutual Information (MI). The FC between each pair of areas was estimated as the FC between (1) the sources closest to their respective centroids or (2) the PCA of all the sources of each area. Areas were defined using both AAL and HO atlases, but since AAL has higher spatial resolution especially in the frontal areas, only the results using AAL are shown here.

Statistical comparisons between groups were performed using two-factor ANOVA test, with the diagnosis and the center where the recording was taken (CTB in Madrid or CBU in Cambridge) as factors. Since FC values do not usually comply with the normality and homoscedasticity hypothesis of the ANOVA test, we calculated the nonparametric statistics by mean of a permutation test, with 100,000 permutations. In order to address the multiple comparisons problem, a False Discovery Rate (FDR) of 10% (Q=0.10) was applied to the results.

Results in Theta band

Both PLV and MI showed differences between the MCI patients and the healthy controls. Several motifs could be identified. In essence, two main results were founded: 1) PLV & MI measurements, using PCA and centroid methods, detected a parieto-occipital increased FC in the MCI group when compared to the CN group. 2) In addition, MI FC values, using the centroid method, showed a fronto-frontal enhanced FC along with a diminished parieto-temporal FC in the MCI group when comparing to healthy controls. See figure 11A and 11B.

Results in Alpha band

Alpha band showed the same significant motif for both PLV (up) and MI (down) FC values using the PCA method. The motif showed a fronto-frontal and fronto-parietal decreased FC in the MCI group when compared to the healthy control group. See figure 11C and 11D.

Results in broadband

MI analyses in broadband showed an increase in connectivity in MCI at a global level, when comparing with the healthy controls. These results appeared both using both the PCA-based (up) and the centroid-based (down) FC. See figure 11E and 11F.

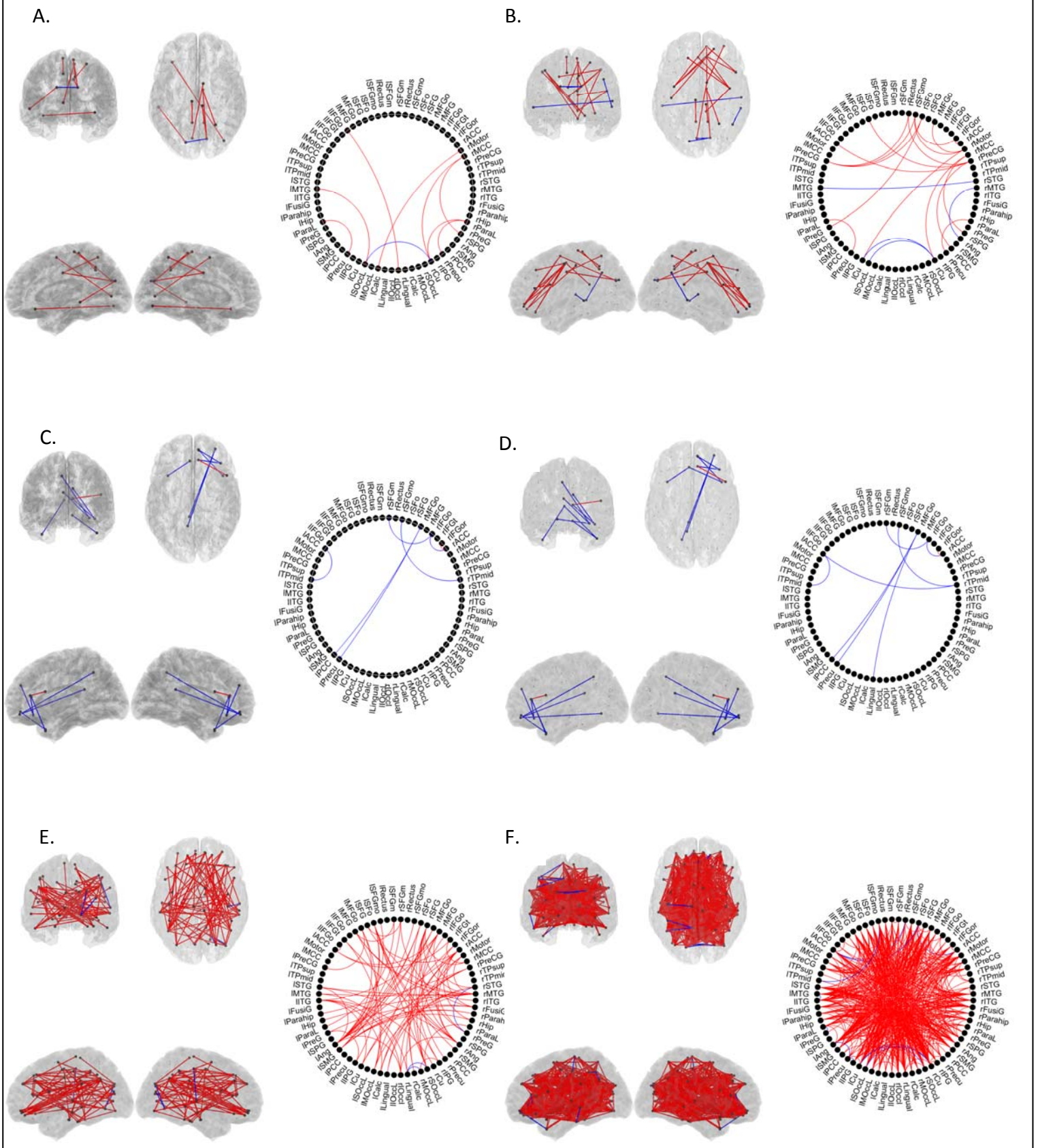

Figure 11. Differences in functional connectivity (PLV and MI) between the MCI patients and the healthy controls within frequency bands. A, Theta band PLV based on centroid areas. B, Theta band MI based on centroids areas; C, Alpha band PLV based on PCA areas; D, Alpha band MI based on PCA areas; E, Broadband MI based on PCA areas; F, Broadband MI based on areas centroids. Red lines: MCI> Controls; Blue Lines Controls>MCI.

OXFORD

The following analyses explore the sensor-space power spectrum and source-space Hidden Markov Model (HMM) analyses on the BioFIND cohort. This is a first pass proof-of-concept analysis designed to demonstrate the effectiveness of the preprocessing pipeline with the sensorspace analysis and the feasibility of HMM analyses on large-scale multi-site datasets. No strong scientific claims are reported from the HMM analyses, rather we show that there is no evidence to suggest that the differences in cohort or acquisition site make HMM analyses impractical.

Materials and methods

MEG Sensorspace Preprocessing

The data are preprocessed using tools from the OHBA Software Library (OSL). This is a Matlab Toolbox that builds upon SPM, Fieldtrip and FSL to provide a range of useful processing and analysis functions.

The analysis begins following the tSSS MaxFilter procedure performed by Cambridge and Madrid. The Maxfiltered data were converted to SPM12 format and was then downsampled to 250Hz and a 1-45Hz bandpass filter applied.

Time segments containing artefacts were detected using an automatic algorithm to ensure reproducibility and avoid user bias that may be introduced by manual artefact detection. Bad segments were rejected by identifying outliers in the standard deviation of the signal computed across all sensors in 1s non-overlapping windows. Outliers were identified using the generalized extreme Studentized deviate method (Rosner, 1983) at a significance level of a 0.05 and with the maximum number of outliers limited to 20% of the data set. The windows corresponding to the outliers were then marked as bad samples in the continuous dataset and excluded from subsequent preprocessing and analysis. Further de-noising was carried out using Independent Components Analysis. This decomposes the sensor space data into a set of statistically independent additive components. Each component is correlated with the EOG and ECG channels and any components with a correlation greater than .5 were marked as ‘bad’ and rejected from the dataset.

Sensor-space General Linear Model

General Linear Modelling was used to explore the sensor space power spectra. These analyses were carried out in OHBA Analysis Tool (OAT). The sensor space data was z-scored

to normalised total spectral power across sensors and participants before being converted into Time-Frequency data using a 5-cycle wavelet transform and the mean power across time modelled with a GLM using a single constant regressor. This first-level regression is repeated for each frequency of each channel for all participants.

Two second-level GLMs are used to summarise the differences in power spectra across participants. Firstly, we perform a contrast between patients and controls across the whole dataset and secondly, we interrogate the effect of MMSE within the patients only.

In the Patient-Control contrast, power is predicted across all datasets using a constant mean regressor along with the participant's diagnostic condition, gender, age and site. Three contrasts are used to summarise the power for Patients, Controls and Patients-Controls. This second-level GLM is repeated for each sensor and each frequency. In the MMSE correlation, power at each sensor and frequency is predicted across the patient datasets using a mean term, regressors for site, gender and age and a parametric regressor coding MMSE score. The contrast of interest isolated the MMSE regressor. Again, this GLM is computed for all frequencies in all sensors.

MEG Sourcespace Preprocessing

Registration between the MEG data and individual structural MRI scans was carried out using RHINO (Registration of Headshapes Including Nose in OSL). This tool uses FSL scalp extraction routines and is designed to make full use of Polhemus TM 3-D digitizer headshape points during the registration. The first stage uses the Polhemus and MRI Fiducials to make an initial registration before the scalp extraction and headshape points are used to fit a more precise registration.

Prior to source modelling, the Magnetometers and Gradiometers are normalised to compensate for their large differences in variance. An eigenvalue decomposition is computed across sensors for each sensor-type and the data are scaled by the smallest eigenvalue. The normalised sensor data is then projected onto a 8mm grid across the brain using an LCMV beamformer. The data covariance in the LCMV beamformer is regularised to a dimensionality of 50 prior to beamforming, partly to compensate for Maxfilter reducing the rank of the sensor data and partly to attenuate the effect of noise on the covariance estimate. Parcel-wise time-courses are estimated using a PCA across all voxels within 39 cortical parcels. The 39 parcel time-courses are then orthogonalised using symmetric multivariate leakage correction to reduce any volume conduction (Colclough et al., 2015)

Hidden Markov Modelling

A Hidden Markov Model is used to describe the network dynamics in the source-space Amplitude Envelope data.

The amplitude envelopes of the parcel time-courses are computed using the Hilbert Transform. The amplitude envelope time-course for each subject and parcel is then demeaned and variance normalised before being concatenated into one group time-course. A 6-state HMM is then inferred on this data. A multivariate Gaussian observation model is used describing the mean and covariance of the envelope data following the methods in Baker et al. (2014) and Vidaurre et al. (2017a).

The HMM inference returns a time course of posterior probabilities, representing the probability that a state is on at each time point. Global statistics about the HMM dynamics are estimated from these attributes. Firstly the average lifetime (also known as the dwell-time) of each state is computed as the average time elapsed between entering and exiting a state. The fractional occupancy is computed across all time within a single participant's dataset as the proportion of time spent in each state. Finally, the interval length is computed as the time elapsed between visits to a state.

The spatial distribution of Envelope Power is extracted from each states observation model by taking the expectation of the mean envelope value for each parcel and state. These values are normalised across parcels within each state to provide a summary of the topology of power.

Group differences in the State Fractional Occupancies are modelled using a General Linear Model (GLM). Six predictors are used to describe individual variation in fractional occupancy for each state, the regressors and contrasts are summarised in figure 12. STDCOPEs are estimated as the square root of the VARCOPE of each COPE and t-statistics are the COPE divided by the STDCOPE.

Permutation statistics are used to establish statistical significance based on the t-statistic for each contrast. 5000 row permutations are used to build a null distribution of COPE statistics and significance was taken to be the 97.5th percentile of this null distribution. This is repeated for the reverse contrast to perform a two-tailed test. Multiple comparisons are corrected by adding the maximum statistic across states to the null distribution at each permutation.

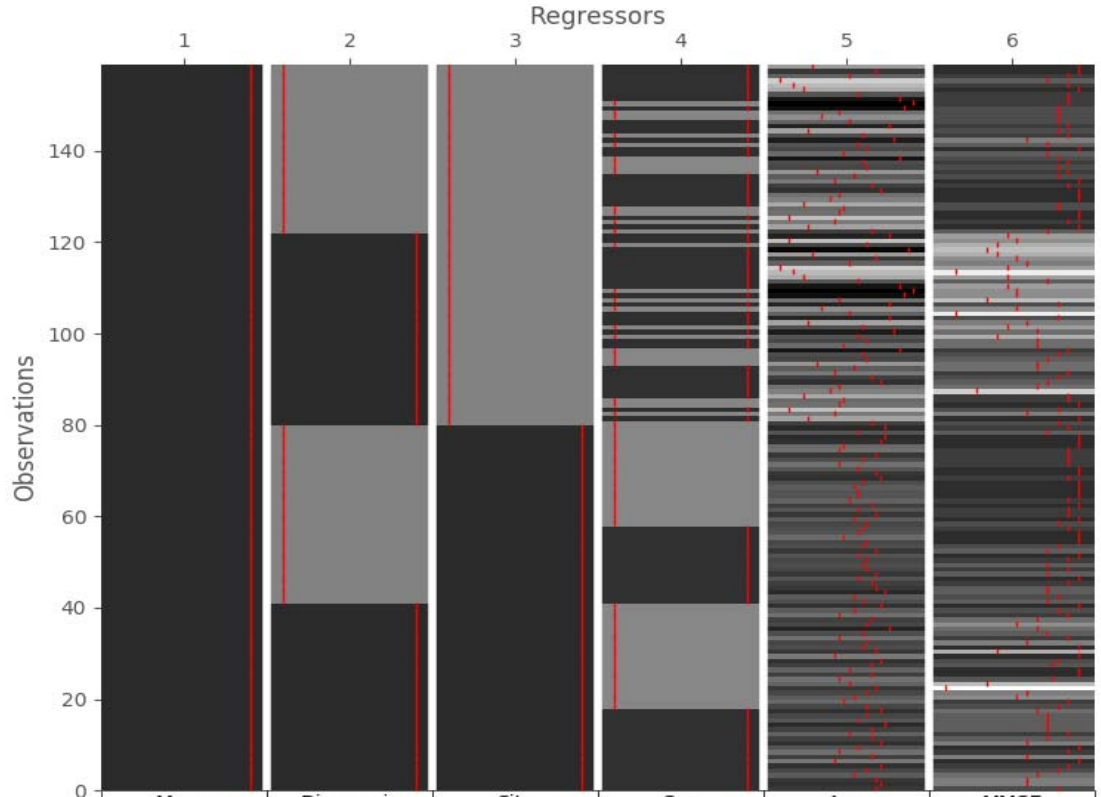

	Mean	Diagnosis	Site	Sex	Age	MMSE
Mean	1.0	0.0	0.0	0.0	0.0	0.0
Madrid>Cambridge	0.0	0.0	1.0	0.0	0.0	0.0
Madrid<Cambridge	0.0	0.0	-1.0	0.0	0.0	0.0
Male>Female	0.0	0.0	0.0	1.0	0.0	0.0
Male<Female	0.0	0.0	0.0	-1.0	0.0	0.0
Age	0.0	0.0	0.0	0.0	1.0	0.0
-Age	0.0	0.0	0.0	0.0	-1.0	0.0

Results

Sensorspace General Linear Model

Figure 13a shows the group Contrast of Parameter Estimates (COPEs) for the mean power in each frequency band averaged across all sensors. Both patients and controls have a strong 1/f type slope across the spectrum and a clear alpha oscillation. The biggest differentiating factor between groups is a shift in the peak frequency of the alpha oscillation, which averages 10Hz for controls and around 7-8Hz for patients. A t-test between the two groups per frequency band shows higher spectral power for patients in low frequency bands (<~8Hz) and controls in higher frequencies (>~8Hz). The group level COPE for each group is shown across sensors in figure 13b and shows that the Alpha effect is more prominent in posterior sensors whilst the frontal sensors are dominated by the 1/f slope and show little group difference.

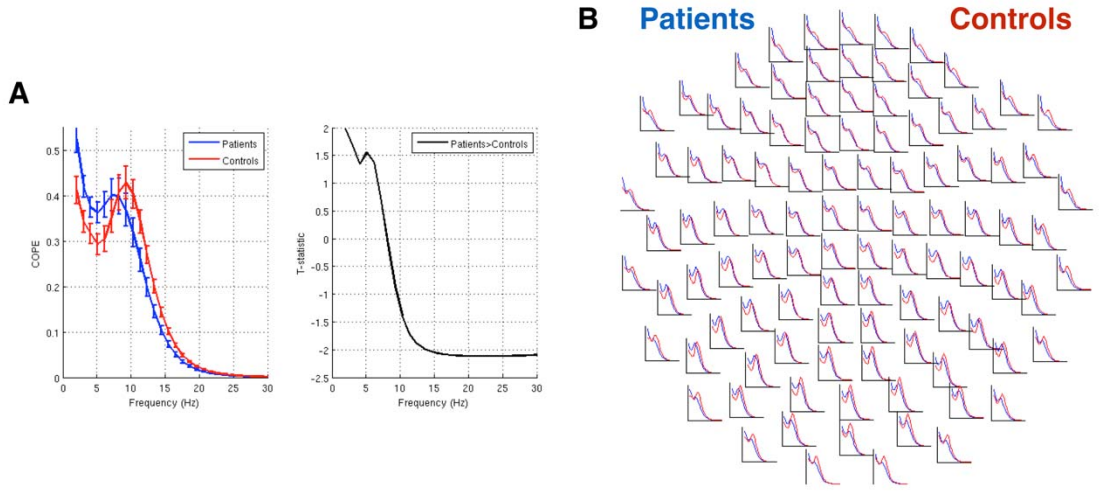

Figure 13. A) The COPEs for the Patient and Control groups for each frequency averaged across sensors and the t-stat for the contrast between them. B) The average COPE for each frequency for each sensor.

Figure 14a shows the distribution of MMSE scores for the patient and control groups. There is a strong ceiling effect for the controls, who all show high (>25) MMSE scores with little variance across participants. In contrast, the patients show a wider spread in MMSE value (95th percentiles are between 18 and 30). As such, we proceed with the MMSE correlation using only the patient values.

The topology of the COPE quantifying the parametric variation between MMSE and spectra power in the alpha bands across patients is shown in figure 14B. The strongest correlations are in the posterior sensors, consistent with the Patient-Control contrast. Finally, the relationship between power at 11Hz and MMSE for a single sensor is shown in figure 14C

with a linear least-squares line of best fit. This shows the positive correlation between MMSE and high (>8Hz) alpha power.

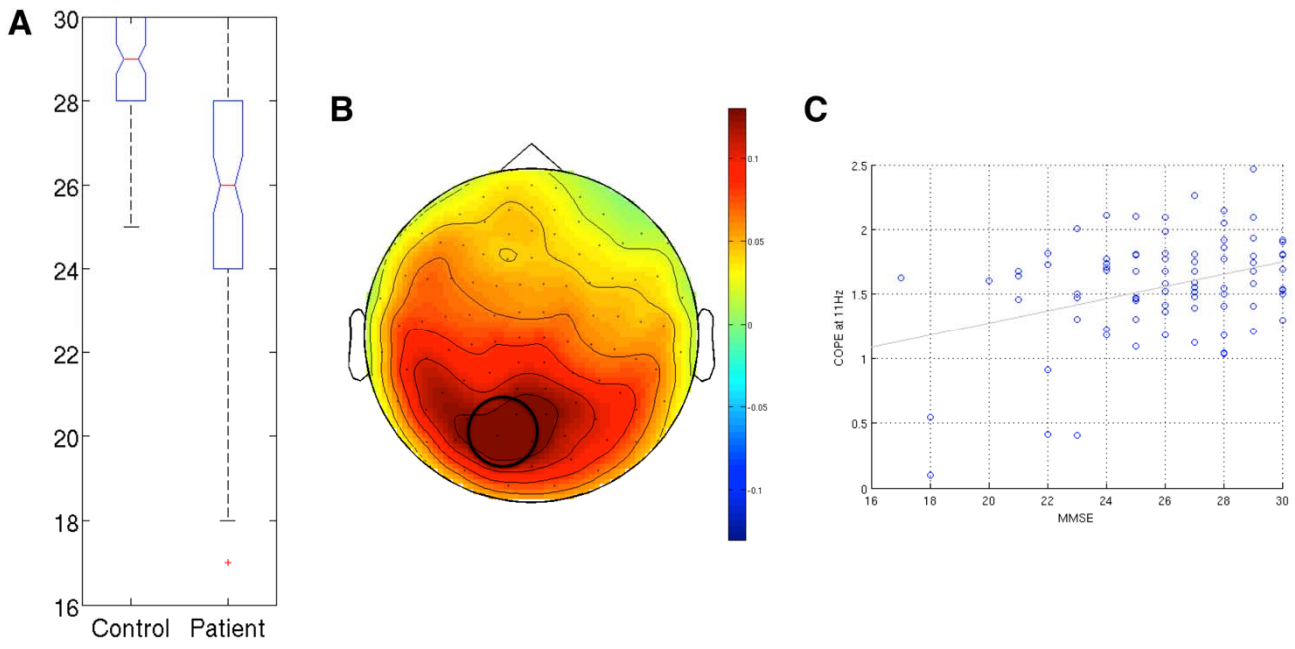

Figure 14. A) The MMSE distributions for the Patient and Control groups. B) The topology of the COPE quantifying the relationship between high alpha power and MMSE for the patient group. The black circle indicates the sensors of interest C) The relationship between high alpha power and MMSE in the sensors of interest indicated in B.

Source-space Hidden Markov Model

The expected power for each parcel in each state is shown in figure 15A. Power is normalised within each state to show the relative topology of power. States 1, 2 and 4 have high envelope values in frontal and frontotemporal regions whilst state 3 is characterised by high envelopes in the motor cortex. Finally, states 5 and 6 show power in occipital regions. The mixing between these states is even across participants and states, though there is some inter-subject variance as seen in figures 15B. Finally, the state lifetimes are around 100-200ms (Figure 4c) and reoccur around every 500-1500ms (Figure 15C,D), consistent with previous applications of the Amplitude Envelope HMM (Baker et al., 2014).

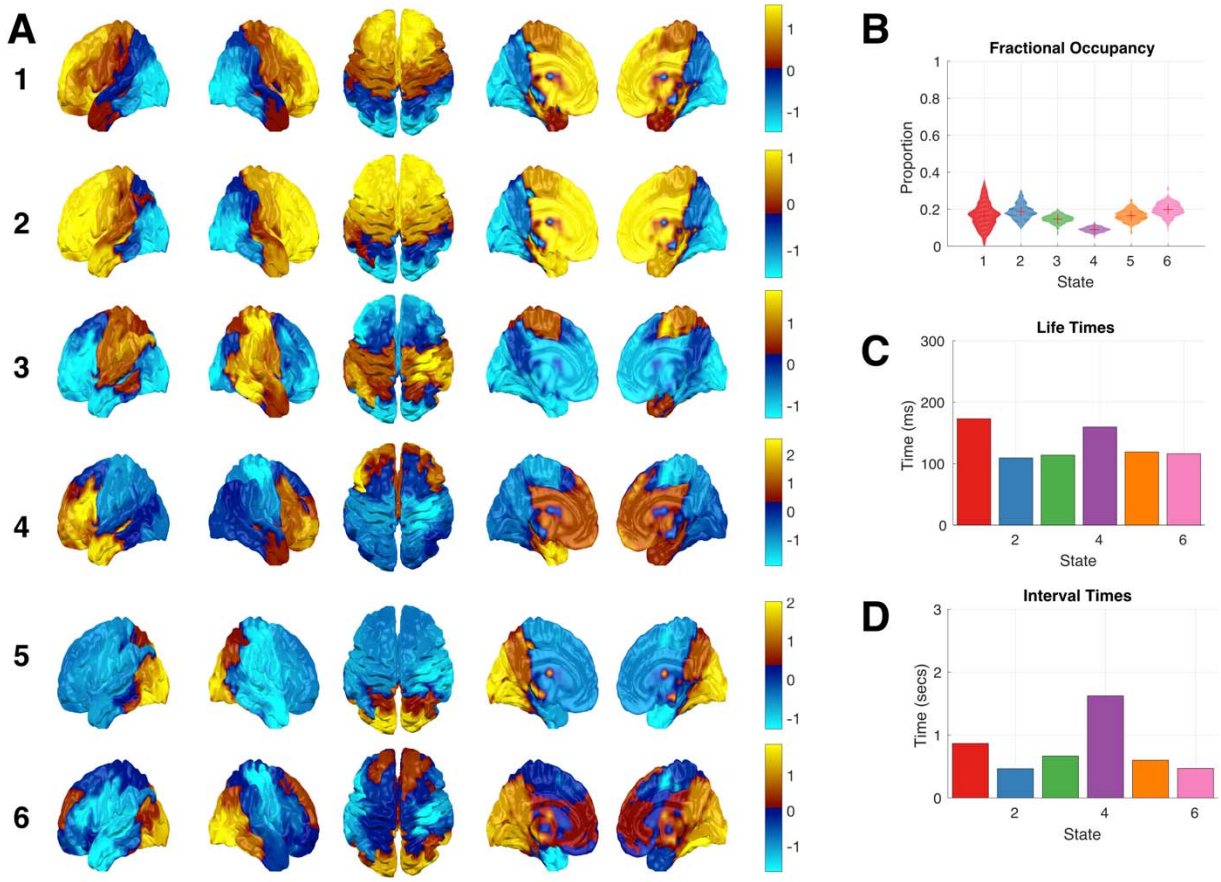

Figure 15. A) The spatial maps describing the areas of high and low envelope power within each of the six states. B) The fractional occupancy distribution across participants for each state. C) The average lifetime of each state. D) The average interval time for each state.

A General Linear Model (GLM) is estimated to describe the individual subject Fractional Occupancy values for each state. The Contrast of Parameter Estimates (COPEs) for the differential contrasts outlined in figure 12 can be seen in figure 15 with STDCOPEs as error bars. The 'Mean' contrast in Figure 16 recovers the mean fractional occupancies of the distributions in figure 15B. The other 3 contrasts quantify sources of variance which we do not straightforwardly relate to MCI or it symptomology: Madrid>Cambridge, Male>Female and Age. No state showed a significant effect of any of these regressors compared to the null distributions.

The HMM is a highly sensitive to changes in the statistical properties of data whether they arise from change in the underlying neuronal dynamics or from change in extraneous noise. For instance, it is common for differences in noise between scan sessions to lead to single states coding for single data runs or specific artefact sources. Here, we show that it is feasible to estimate the HMM on large multi-site datasets without the acquisition

differences dominating the outcome. Rather, we see that the HMM is able to identify a range of interpretable states which mix well across all scan sessions. A further exploration of the diagnostic condition and MMSE values would be feasible given these results.

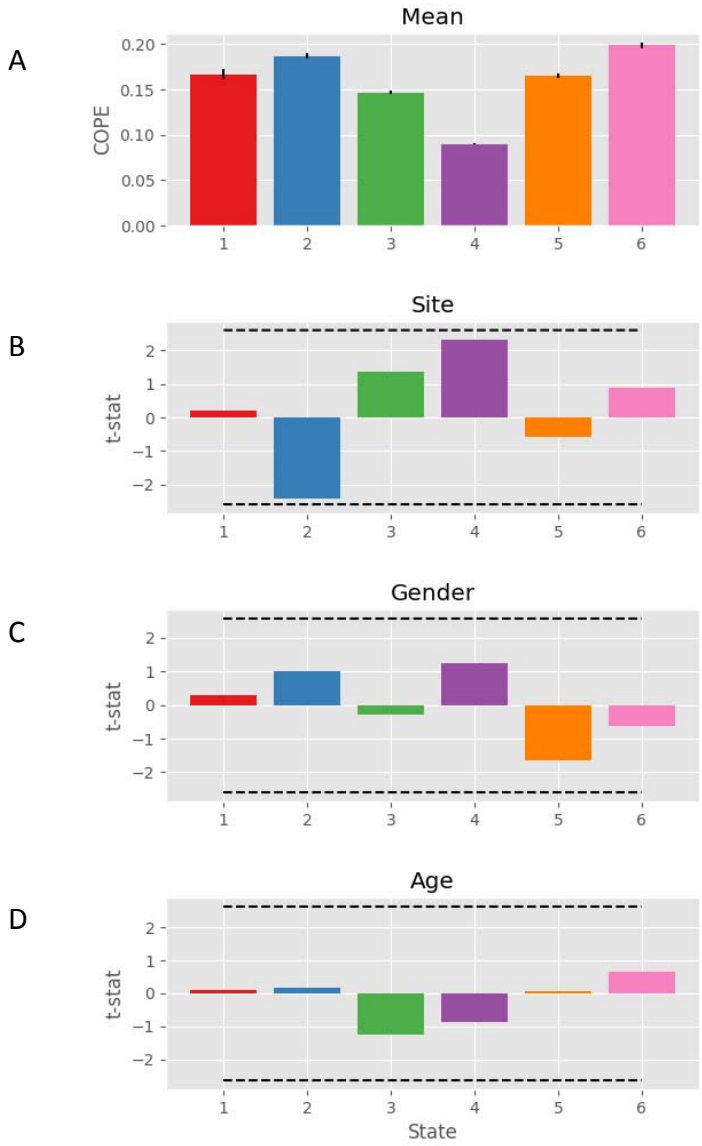

Figure 16. The results of the GLM on the HMM Fractional Occupancy scores. A) The COPE for the mean fractional occupancies, these are the same as the mean values in figure 4b. B) The t-stats for the contrast between the two acquisition sites. Dotted lines indicate null permutation significance critical values from the positive and negative contrasts. C) The t-values for Gender. D) The t-values for Age.

Outcome summary & Framework of Recommendations

The working group achieved the main goals specified in the protocol by creating a consensus methodological framework for assessing MEG indices of MCI/AD, and using this framework to form a database of multicentre results and a pipeline for preprocessing and statistical analyses that identified several reliable MEG markers of MCI. The specificity of the results is to be examined in further analyses that compare additional patient groups (including frontotemporal dementia).

The details of the paradigm, data acquisition and preprocessing are included in Table 3 below.

MEG database summary

The database combined resting state data from patients and controls acquired in Madrid, Cambridge and Oxford. Collating and merging the data highlighted a few key issues, some specific to MEG but also involved generic hurdles for multisite studies. For example, data sharing requires multiple permissions from research ethics committees and site approvals to transfer and allow access to data. In the database, only compatible datasets were included (in terms of hardware, paradigms and participants) that could be directly compared. Although there were still site differences demonstrating the need to include site as a covariate in the analyses, the analyses do show that acquisition differences did not dominate the outcome.

MEG analyses summary

The analyses demonstrated the sensitivity of MEG to disease, with changes in cortical oscillations identified as a key feature of MCI. Scalp-frequency images could classify patients and controls with 71% accuracy, comparable to using the MRI or MMSE (75% and 81%, respectively), and together with the MRI improved classification to 79%. The sensitivity of MEG is clear, especially considering that the MRI and MMSE are not independent measures for classification, as both are used in the diagnostic decision.

Frequency specific abnormalities evident in the patient group included increased power in lower frequencies (2-8Hz), a decrease in higher frequencies (12Hz+), and a downward shift in peak alpha frequency that correlated with MMSE scores. A decrease in alpha power (6/8-12Hz) in the patient group was dependent on whether the data were normalised. Theta power was the most sensitive to classification, with 71% accuracy for both sensor types.

Localisation of these frequency changes was prominent across widespread bilateral temporal structures.

Functional connectivity was also sensitive to frequency specific changes in MCI: In frontal regions connectivity was enhanced in the theta band, but diminished in the alpha band, and connectivity to posterior regions was reduced in both bands.

The results reveal oscillatory signatures that are sensitive to disease, have the potential to further understanding of the mechanisms of degeneration and conversion from MCI to AD, and to provide a benchmark for future studies, including validation of new experiments, comparing with other types of neurodegeneration, examining prodromal genetically susceptible individuals, and for assessments of therapeutic treatments.

MEG acquisition and procedures summary

Table 3. Multisite data acquisition and data sharing protocols for a short '5 minute-eyes closed' resting state paradigm.

Data Sharing	Anonymised data	Individuals were not identifiable from MEG / MRI data. For example, no PID in data sets, defacing of MRI's.
	Research Ethics Committee	Ethical committee approved data sharing beyond the team acquiring the data.
	Site approval	Documents set up to approve transfer of data between sites according to site specific administrative procedures.
Hardware	Elekta Neuromag	Current study includes data only from Elekta neuromag, but protocol could be extended to other systems.
Paradigm	Acquisition instructions	Participants instructed "Please close your eyes and keep them closed and try to relax and stay still for the duration of the recording. This will take about five minutes, please stay awake".
	Acquisition procedures	Data acquired at 1Khz for at least 5 minutes. Instructions and recording time are limited to reduce discomfort or confusion in patients.
	Time of acquisition	Times kept consistent to midmorning / early afternoon.

Participants	Sample size	Sufficient numbers from each site to include site effects as covariates (84 patients and controls from Cambridge and 84 from Madrid).
	Patients and Controls	Healthy controls compared between sites to examine compatibility of data and site effects.
	Demographics	Age range, disease stage and duration similar across site groups.
	State during MEG acquisition	Resting state acquired as first paradigm in session, or at least not having completed other cognitive or learning paradigms immediately prior.
	MRIs	T1 structural MRIs acquired for all participants.

Preprocessing pipeline

Proposed pipeline for MEG data analysis (BioFIND project) (v2, 13/01/2017)

Background

This pipeline is based on the results post-meeting discussing of the initial BioFIND workshop that took place at Trinity Hall, Cambridge University, on Nov. 7-8. It is intended to be a unified pipeline for the (pre)processing of MEG data for its use as a potential biomarker of dementia. It is also, at least partially, based on the pipeline agreed for the members of the MAGIC-AD consortium, as presented in Maestú *e t al.*, Neuroimage Clin. 2015; 9: 103–9.

Steps of the pipeline

1. Recordings

As described in Table 3.

2. Preprocessing

2.1. *Maxfilter*. We propose to apply tSSS (as implemented in MaxFilter v2.2) with movement compensation, if available.
As for the bad detection channel, there are two options. The first one consists in using automatic bad channel rejection using the Cambridge's scripts. The second will be to use a manual procedure. Both options have obviously pros and cons. The former one is faster and much easier to replicate. The second one requires more work and is up to some point, group dependent, yet it allows likely cleaner data.
The script and parameters for the tSSS filtering are as follows:

```
# Processing file namefile
echo Processing file\: namefile
date +'%d/%m/%Y %H:%M:%S.%N' >> /neuro/data/Logs/namefile.log
echo Processing file\: namefile >> /neuro/data/Logs/namefile.log
echo Bad files\: 000 000 000 000 000 000 000 000 000 000 >> /neuro/data/Logs/namefile.log
```

```
echo >> /neuro/data/Logs/namefile.log
date +'%d/%m/%Y %H:%M:%S.%N' >> /neuro/data/Errs/namefile.err
echo Processing file\: namefile >> /neuro/data/Errs/namefile.err
echo >> /neuro/data/Errs/namefile.err
a=`nice /neuro/bin/util/maxfilter -gui -f /opt/neuromag/data/namefile.fif -origin fit -frame head`
[[ $a =~ \#o\ head\ \(-?[0-9\.]+\)\ \(-?[0-9\.]+\)\ \(-?[0-9\.]+\)\ mm ]]
a1=${BASH_REMATCH[1]}; a2=${BASH_REMATCH[2]}; a3=${BASH_REMATCH[3]}
echo Origin found in $a1 $a2 $a3 >> /neuro/data/Logs/namefile.log
echo >> /neuro/data/Logs/namefile.log
nice /neuro/bin/util/maxfilter -gui -f /opt/neuromag/data/namefile.fif -o /opt/neuromag/data/namefile_tsss.fif -origin
$a1 $a2 $a3 -frame head -cal /neuro/databases/sss/sss_cal.dat -bad 000 000 000 000 000 000 000 000 000 000
-st 10 -corr 0.9 -hpiwin 200 -hpistep 10 -hpicons -hpisubt off -format short -force -st inter 1>>
/neuro/data/Logs/namefile.log 2>> /neuro/data/Errs/namefile.err
echo >> /neuro/data/Logs/namefile.log
echo >> /neuro/data/Logs/namefile.log
echo >> /neuro/data/Errs/namefile.err
echo >> /neuro/data/Errs/namefile.err
```

2.2. Application of an automatic artefact detection: blinks, jumps and muscle. We propose to use the standard FieldTrip pipeline for this purpose.

2.3. Segmentation of the data in 4 seconds segments, with additional 2 s. padding at both edges to account for edge effects when using the HT later on the pipeline (in our experience the best quality/cost ratio in order to ensure enough low frequency resolution and number of clean trials) dismissing those artifacted fragments.

2.4. ICA: since we are working with eyes closed records, the most straightforward option seems to be not to apply any ICA, which is also the simplest option.

3. Source reconstruction

3.1. We agreed to use:

- Single shell head model
- LCMV beamformers combining information from both gradiometers and magnetometers (the Oxford group scripts based on SPM). We use 1 cm spacing for the voxels, which results in around 2459 distributed sources (-1 cm of inward parameter).
- We use a MNI template where we define the grid. Then, we transform this grid to the subject space as detailed in the Fieldtrip webpage: " *http://www.fieldtriptoolbox.org/example/create_single-subject_grids_in_individual_head_space_that_are_all_aligned_in_mni_space"*

3.2 On the anatomical parcellation and the choice of a representative time series from each ROI, the consensus was to try two different options in each case, as follows:

- Parcellation atlas: we decided to try AAL and Oxford-Harvard. We use a modified Oxford-Harvard, which typically contains 64 ROIs (around 60 cortical ones plus amygdala and hippocampus).
- Representative time series: here we will check the use of the first PCA (as Oxford does) and the center voxel (Amsterdam's approach).

This results in 2x2=4 different sets of ROIs time series to test.

Terminology

AAL: automatic anatomical labeling atlas
AD: Alzheimer's Disease
COPE: contrast of parameter estimate
CSF: cerebrospinal fluid
FC: functional connectivity
FTLD: frontotemporal lobar degeneration
Grad: gradiometers
GM: gray matter
GLM: general linear model
HMM: Hidden Markov Model
MAG: magnetometers
MCI: mild cognitive impairment
MEG: magnetoencephalography
MI: mutual information
MMSE: Mini Mental State Exam
MRI: magnetic resonance imaging
PCA: principal component analysis
PLV: phase locking value
WM: white matter

Contributors

Laura Hughes (coordinator), Department of Clinical Neurosciences, University of Cambridge, UK and MRC Cognition and Brain Sciences Unit, University of Cambridge, UK
Rik Henson, MRC Cognition and Brain Sciences Unit, University of Cambridge, UK
James Rowe, Department of Clinical Neurosciences, University of Cambridge, UK and MRC Cognition and Brain Sciences Unit, University of Cambridge, UK
Fernando Maestú, Laboratory of Cognitive and Computational Neuroscience (UCM-UPM), Centre for Biomedical Technology, Madrid, Spain; Biomedical Research Networking Center in Bioengineering Biomaterials and Nanomedicine (CIBER-BBN), Madrid, Spain; and Department of Basic Psychology II, Faculty of Psychology, Universidad Complutense de Madrid, Madrid, Spain.
Ernesto Pereda, Laboratory of Cognitive and Computational Neuroscience (UCM-UPM), Centre for Biomedical Technology, Madrid, Spain; and Department of Industrial

Engineering, Instituto Universitario de Neurociencia, Universidad de La Laguna, Tenerife, Spain.

Ricardo Bruña, Laboratory of Cognitive and Computational Neuroscience (UCM-UPM), Centre for Biomedical Technology, Madrid, Spain; Biomedical Research Networking Center in Bioengineering Biomaterials and Nanomedicine (CIBER-BBN), Madrid, Spain.

Kia Nobre, Oxford Centre for Human Brain Activity, University of Oxford, Oxford, United Kingdom; and Department of Experimental Psychology, University of Oxford, Oxford, United Kingdom

Mark Woolrich, Oxford Centre for Human Brain Activity, University of Oxford, Oxford, United Kingdom

Andrew Quinn, Oxford Centre for Human Brain Activity, University of Oxford, Oxford, United Kingdom

Arjan Hillebrand, VU University Medical Center, Amsterdam, The Netherlands.

Alida Gouw, VU University Medical Center, Amsterdam, The Netherlands.

Jyrki Mäkelä, BioMag Laboratory, HUS Medical Imaging Center, Helsinki University Central Hospital, Helsinki, Finland.

References

Bajo, R., Maestú, F., Nevado, A., Sancho, M., Gutiérrez, R., Campo, P., Castellanos, N.P., Gil, P., Moratti, S., Pereda, E., Del-Pozo, F., (2010) Functional connectivity in mild cognitive impairment during a memory task: implications for the disconnection hypothesis. *J Alzheimers Dis*. 22(1):183-93.

Bajo, R., Castellanos, N.P., Cuesta, P., Aurtenetxe, S., Garcia-Prieto, J., Gil-Gregorio, P., del-Pozo, F., Maestu, F., (2012) Differential patterns of connectivity in progressive mild cognitive impairment. *Brain Connect*. 2(1):21-4

Baker, A.P., Brookes, M.J., Rezek, I.A., Smith, S.M., Behrens, T., Probert Smith, P.J., Woolrich, M., (2014). Fast transient networks in spontaneous human brain activity. eLife 25;3:e01867

Colclough, G.L., Brookes, M.J., Smith, S.M., Woolrich, M.W., (2015). A symmetric multivariate leakage correction for MEG connectomes. *NeuroImage* 117, 439– 448.

de Haan, W., Pijnenburg, Y.A., Strijers, R.L., van der Made, Y., van der Flier, W.M., Scheltens, P., Stam ,C.J., (2009) Functional neural network analysis in frontotemporal dementia and Alzheimer's disease using EEG and graph theory. *BMC Neurosci*. 21;10:101

Garcés, P., Vicente, R., Wibral, M., Pineda-Pardo, J.Á., López, M.E., Aurtenetxe, S., Marcos, A., de Andrés, M.E., Yus, M., Sancho, M., Maestú, F., Fernández, A. Brain-wide slowing of spontaneous alpha rhythms in mild cognitive impairment. Front. Aging Neurosci. 5, 1–7 (2013).

Gouw, A.A., Alsema, A.M., Tijms, B.M., Borta, A., Scheltens, P., Stam, C.J., van der Flier, W.M. (2017) EEG spectral analysis as a putative early prognostic biomarker in nondemented, amyloid positive subjects. Neurobiol Aging. 57:133-142.

Hillary, F.G., Roman, C.A., Venkatesan, U., Rajtmajer, S.M., Bajo, R., Castellanos, N.D., (2015) Hyperconnectivity is a fundamental response to neurological disruption. *Neuropsychology*. 29(1):59-75.

Hughes, L.E, Ghosh, B.C., Rowe, J.B., (2013) Reorganisation of brain networks in FTD and PSP. *Neuroimage Clin*. 2:459-468.

Hughes L.E., Rowe J.B. (2013) The impact of neurodegeneration on network connectivity: a study of change detection in frontotemporal dementia. *J Cogn Neurosci*. 25(5):802-13.

López, M.E., Cuesta, P., Garcés P., Castellanos, P.N., Aurtenetxe, S., Bajo, R., Marcos, A., Delgado, M.L., Montejo, P., López-Pantoja, J.L., Maestú, F., Fernandez, A. (2014) MEG spectral analysis in subtypes of mild cognitive impairment. *Age (Dordr).* 36(3):9624.

López-Sanz, D., Bruña, R., Garcés, P., Camara, C., Serrano, N., Rodríguez-Rojo, I.C., Delgado, M.L., Montenegro, M., López-Higes, R., Yus, M., Maestú, F. (2016) Alpha band disruption in the AD-continuum starts in the Subjective Cognitive Decline stage: a MEG study. Sci Rep. 24;6:37685.

Maestú F, et al., (2015) A multicenter study of the early detection of synaptic dysfunction in Mild Cognitive Impairment using Magnetoencephalography-derived functional connectivity. *Neuroimage Clin*.1;9:103-9.

Rosner, B., (1983). Percentage Points for a Generalized ESD Many-Outlier Procedure. Technometrics 25, 165–172.

Stam, C.J., Jones, B.F., Manshanden, I., van Cappellen van Walsum, A.M., Montez, T., Verbunt, J.P., de Munck, J.C., van Dijk, B.W., Berendse, H.W., Scheltens, P., (2006) Magnetoencephalographic evaluation of resting-state functional connectivity in Alzheimer's disease. *Neuroimage*; 32(3):1335-44

Stam, C.J., de Haan, W., Daffertshofer, A., Jones, B.F., Manshanden, I., van Cappellen van Walsum , A.M., Montez, T., Verbunt, J.P., de Munck, J.C., van Dijk, B.W., Berendse, H.W., Scheltens P., (2009) Graph theoretical analysis of magnetoencephalographic functional connectivity in Alzheimer's disease. *Brain*;132(Pt 1):213-24.

Vidaurre, D., Abeysuriya, R., Becker, R., Quinn, A.J., Alfaro-Almagro, F., Smith,
S.M., Woolrich, M.W., (2017a). Discovering dynamic brain networks from big data in rest and task. NeuroImage.

Zamrini, E., Maestu, F., Pekkonen, E., Funke, M., Makela, J., Riley, M., Bajo, R., Sudre, G., Fernandez, A., Castellanos, N., Del Pozo, F., Stam, C.J., van Dijk, B.W., Bagic, A., Becker, J.T., (2011) Magnetoencephalography as a putative biomarker for Alzheimer's disease. *Int J Alzheimers Dis*. 10;2011:280289